Triple sulfur isotope relationships during sulfate-driven anaerobic oxidation of methane

Shanggui Gong[a,g], Yongbo Peng[b,*], Huiming Bao[b,*], Dong Feng[a,c], Xiaobin Cao[b], Peter Crockford[d,e], Duofu Chen[f]

[a] *CAS Key Laboratory of Ocean and Marginal Sea Geology, South China Sea Institute of Oceanology, Chinese Academy of Sciences, Guangzhou 510301, China*

[b] *Department of Geology and Geophysics, Louisiana State University, Baton Rouge, LA 70803, USA.*

[c] *Laboratory for Marine Mineral Resources, Qingdao National Laboratory for Marine Science and Technology, Qingdao 266071, China*

[d] *Department of Earth and Planetary Sciences, Weizmann Institute of Science, Rehovot Israel*

[e] *Department of Geoscience, Princeton University, Princeton NJ 08544 USA*

[f] *Hadal Science and Technology Research Center, College of Marine Sciences, Shanghai Ocean University, Shanghai 201306, China*

[g] *University of Chinese Academy of Sciences, Beijing 100049, China.*

∗Corresponding authors.

E-mail addresses: ypeng@lsu.edu (Y.B. Peng); bao@lsu.edu (H.M. Bao).

Abstract

Sulfate-driven anaerobic oxidation of methane (SD-AOM) plays a critical role in regulating the global methane budget. Determination of the diagnostic triple isotope exponent $^{33}\theta$ ($\equiv \ln^{33}\alpha / \ln^{34}\alpha$) for SD-AOM can help to identify and quantify microbial sulfate reduction via SD-AOM in the environment. The history of Earth's surface redox conditions can also be examined through the measurement of triple sulfur isotope compositions in sedimentary rocks. Due to difficulties in both culturing anaerobic methanotrophs and sampling pore-water sulfate in SD-AOM-dominated environments, however, the $^{33}\theta$ values for the processes of SD-AOM have not been constrained. We propose that a set of modern cold-seep associated barite samples with low $\Delta\delta^{18}O/\Delta\delta^{34}S$ values bear a record of residual pore-water sulfate during SD-AOM, and therefore the triple sulfur isotope composition of these barites can be used to deduce $^{33}\theta$ values. We applied a 1-D diagenetic reaction-transport model to fit $\Delta^{33}S$ and $\delta'^{34}S$ results from modern cold seep barites collected from five sites in the Gulf of Mexico. Based on revealed negative correlations (R^2=0.77) between $\Delta^{33}S$ and $\delta'^{34}S$ values we calculated an upper-limit $^{33}\theta$ value of 0.5100 to 0.5112 (±0.0005) given a $1000\ln^{34}\alpha$ value of -30‰ to -10‰. This $^{33}\theta$ value is distinctively lower than that of organoclastic sulfate reduction (OSR) in marine environments where the diagnostic isotope fractionation ($1000\ln^{34}\alpha$) is typically more negative than that of SD-AOM. In addition, cold seep barite data display a negative $\Delta^{33}S$-$\delta'^{34}S$ correlation whereas pore-water sulfates of all OSR-dominated settings show a positive one. Therefore, the diagnostic triple-sulfur isotope exponent and associated negative $\Delta^{33}S$-$\delta'^{34}S$

correlation may allow for the identification of SD-AOM in sedimentary records.

Keywords: isotope fractionation; reaction-transport model; cold seeps barite; anaerobic methane oxidation; Gulf of Mexico; multiple sulfur isotopes

1. Introduction

Microbial dissimilatory sulfate reduction coupled with anaerobic methane oxidation (AOM) or sulfate-driven AOM (SD-AOM) has been identified as the main process consuming methane in subsurface seafloor environments (e.g., Reeburgh, 2007; Eggers et al., 2018). Sulfate reduction rates in methane-seep sediments can be several orders of magnitude higher than those measured in non-seep sediments (Aharon and Fu, 2000; Joye et al., 2004). The activity of SD-AOM signifies chemosynthesis-dependent life (Campbell 2006; Kaim et al., 2014), is relevant to greenhouse gas budgets in the geologic past (Olson et al., 2016), and is a major part of the marine carbon cycle (e.g., Peckmann and Thiel, 2004; Zhou et al., 2016). Today one of the most distinct geological features of SD-AOM activity is extremely negative $\delta^{13}C$ value in carbonate rock, typically less than -30‰ (VPDB), (e.g., Peckmann and Thiel 2004; Feng et al., 2016). However, the $\delta^{13}C$ of carbonates is controlled by the mixing ratio of SD-AOM sourced CO_3^{2-} and seawater DIC. High seawater [CO_3^{2-}] and/or low seawater [SO_4^{2-}] that characterizes seawater through much of the Precambrian may have decreased the fraction of SD-AOM sourced CO_3^{2-}, which would have resulted in highly negative $\delta^{13}C$ values preserved in marine carbonate

records far less likely to form prior to the early Paleozoic Era (Bristow and Grotzinger 2013).

It has been observed that coupled $\delta^{18}O$ and $\delta^{34}S$ values of modern pore-water sulfate at different depths in marine sediment cores will bear a typical slope of >0.70 where microbial dissimilatory sulfate reduction is dominated by organotrophic sulfate reduction (OSR) (Aharon and Fu et al., 2000; Antler et al., 2014). Recently, studies of both modern and ancient environments associated with significant SD-AOM have revealed a distinctively lower $\delta^{18}O$-$\delta^{34}S$ slope that ranges from 0.27-0.50 among cold-seep barite and carbonate samples (in the form of carbonate-associated sulfate; Feng and Roberts, 2011; Antler et al., 2015; Feng et al., 2016). This finding offers a potential proxy for SD-AOM activity in geological history. However, the interpretation of $\delta^{18}O$-$\delta^{34}S$ slopes has important caveats. First, the $\delta^{18}O$-$\delta^{34}S$ slope is also dependent on the $\delta^{18}O$ value of seawater sulfate and that of seawater sulfate (Turchyn et al., 2010; Feng et al., 2016; Antler et al., 2017), which has likely changed through Earth history (Claypool, 1980). Second, the slope could be altered if early or late-stage diagenetic processes altered the $\delta^{18}O$ of initially deposited sulfate (Fichtner et al., 2017).

The relationship among triple sulfur isotope compositions (^{32}S, ^{33}S, ^{34}S) of sulfur-bearing compounds can be a diagnostic parameter for SD-AOM activity that is potentially more robust that interpretations solely based on $\delta^{18}O$-$\delta^{34}S$ slopes. Pure cultures of sulfate-reducing microbes with non-methane electron donors have demonstrated a negative correlation between $1000\ln^{34}\alpha$ and $^{33}\theta$ values, i.e. the $^{33}\theta$

increases when the $1000\ln^{34}\alpha$ becomes more negative as a cell-specific sulfate reduction rate decreases (Sim et al., 2011b; Leavitt et al., 2013). Here, $^{33}\theta \equiv \ln^{33}\alpha/\ln^{34}\alpha$, $^{3i}\alpha$ is the diagnostic fractionation factor, defined as $^{3i}R_{H_2S}/^{3i}R_{SO_4^{2-}}$, where ^{3i}R is the ratio of $^{3i}S/^{32}S$, and the superscript '3i' refers to 33 or 34. This positive correlation was suggested to reflect a first order rate difference between sulfate uptake by the cell and sulfate leakage out of the cell during microbial dissimilatory sulfate reduction (Wu and Farquhar, 2013). Since the $1000\ln^{34}\alpha$ was shown to be much negative during SD-AOM than during OSR processes in marine sediments (Aharon and Fu, 2003; Deusner et al., 2014), we expect that the diagnostic $^{33}\theta$ value for SD-AOM should consequently be smaller than that of typical OSR processes in marine environments.

This perceived difference in minor sulfur isotope fractionation between SD-AOM and OSR processes is expected to be manifested in their $\Delta^{33}S$-$\delta'^{34}S$ trajectories of their residues or products. Here, $\Delta^{33}S$ values are the deviation of $\delta'^{33}S$ values from a reference line defined as $\Delta^{33}S \equiv \delta'^{33}S - 0.515 * \delta'^{34}S$, where $\delta'^{3i}S = \ln(1+\delta^{3i}S)$, $\delta^{3i}S = {}^{3i}R/{}^{3i}R_{ref} - 1$, and $^{3i}R_{ref}$ is the abundance ratio of the ^{3i}S and ^{32}S in the sulfur reference standard. For example, according to a linear fit of published $1000\ln^{34}\alpha$ and $^{33}\theta$ values (cf. Ono et al., 2012) and the known $1000\ln^{34}\alpha$ range associated with SD-AOM processes, i.e., -40‰ to -10‰ (Aharon and Fu 2000; Deusner et al., 2014; Sivan et al., 2014), the $^{33}\theta$ value during SD-AOM could be lower than 0.5125. Therefore, the corresponding $\Delta^{33}S$-$\delta'^{34}S$ relationship for SD-AOM dominated pore-water sulfate profiles would exhibit a negative correlation. We predict that such

111 a trajectory could be distinct from the positive $\Delta^{33}S$-$\delta'^{34}S$ correlation reported for
112 OSR-dominated pore-water sulfate profiles (e.g. Strauss et al., 2012; Pellerin et al.,
113 2015; Masterson et al., 2018). If confirmed, the $\Delta^{33}S$-$\delta'^{34}S$ relationship preserved in
114 the sedimentary record is a potentially useful tool for distinguishing different sulfate
115 reduction pathways.

116 More specificity beyond our hypothesis of a different $\Delta^{33}S$-$\delta'^{34}S$ relationships for
117 pore-water sulfate profiles between SD-AOM- and OSR-dominated sediments is not
118 available at this time. Culture experiments show that the $^{33}\theta$ value has a wide range
119 from 0.5079 to 0.5144 (e.g. Sim et al., 2011b; Leavitt et al., 2013). The activity of
120 respiratory enzymes, which is both electron-donor- and strain-specific, influences the
121 degree of sulfur isotope fractionation or the $1000\ln^{34}\alpha$ value (e.g. Sim et al., 2011b;
122 Wing and Halevy 2014; Bradley et al., 2016). Therefore, our first step, should be to
123 calibrate the $\Delta^{33}S$-$\delta'^{34}S$ relationship for a pore-water sulfate profile in a typical
124 SD-AOM-dominated sedimentary setting in a modern marine environment.

125 Due to high sulfate reduction rates in SD-AOM settings, pore-water sulfate
126 concentrations often rapidly decrease at shallow depths (Aharon and Fu, 2000).
127 Top-layers of a sediment cores can easily be disturbed during coring, causing
128 pore-water sulfate to be contaminated by seawater sulfate. In addition, low sulfate
129 concentrations often make it difficult to collect enough pore-water sulfate for triple
130 sulfur isotope analysis. Fortunately, modern cold-seep barite samples have been found
131 to preserve the original isotope signals of pore-water sulfate associated with SD-AOM
132 activity, as demonstrated by their lower $\delta^{18}O$-$\delta^{34}S$ slopes (Feng and Roberts, 2011;

Antler et al., 2015). The other important reason that we sample natural SD-AOM systems is the difficulty in culturing anaerobic methanotrophs (e.g., Girguis et al., 2003). Therefore, to calibrate $^{33}\theta$ and explore the $\Delta^{33}S$-$\delta'^{34}S$ relationship associated with SD-AOM processes, our approach is to measure triple sulfur isotope compositions of modern seep barite samples and use a 1-D diagenetic reaction-transport model to fit a set of $\Delta^{33}S$ and $\delta'^{34}S$ values to deduce a diagnostic $^{33}\theta$ value for SD-AOM dominated settings. Using a $\Delta^{33}S$-$\delta'^{34}S$ correlation instead of a $\delta'^{33}S$-$\delta'^{34}S$ correlation we can improve the data resolution because $\Delta^{33}S$ values have a much higher analytical accuracy than any individual $\delta'^{33}S$ or $\delta'^{34}S$ measurements.

2. Material and method

Barite samples from 5 different cold seep sites in the Gulf of Mexico continental slope (Fig. 1) were collected using a variety of submersibles and remotely operated vehicles. The samples were previously described (Feng and Roberts, 2011). Powdered aliquots were dissolved in 1 mM HCl solution to remove water leachable and acid leachable sulfates. $BaSO_4$ was extracted from the residues and further purified using a DDARP method (Bao, 2006). In brief, the residues after acid treatment were dissolved by a mixed DTPA (a chelating reagent) and NaOH solution. The obtained solution was filtered through a 0.22 μm polycarbonate filter and then acidified with 10M HCl droplets to ~pH=2 to induce $BaSO_4$ precipitation. Droplets of $BaCl_2$ solution were added to ensure full precipitation of SO_4^{2-} as $BaSO_4$. The precipitated $BaSO_4$ was re-dissolved and re-precipitated via another round of the DDARP method.

After bathing in a 3M NaOH solution at 90°C for >40 hours, the wash-cleaned and dried $BaSO_4$ was measured for its $\delta^{18}O$ value at Louisiana State University (LSU) via CO gas generated by a Thermal Conversion Elemental Analyzer (TCEA) at 1430 °C coupled with an isotope-ratio mass spectrometer (MAT 253) in continuous-flow mode. For the analysis of triple sulfur isotope compositions (i.e., $\delta^{34}S$ and $\Delta^{33}S$), ~10 mg of the barite precipitates were reduced to sulfide using a Thode solution at ~100˚C (Thode et al., 1961). The generated H_2S gas was carried by N_2 gas stream and bubbled into a zinc acetate solution that converted H_2S gas to ZnS solid. ZnS was then reacted with $AgNO_3$ to convert to Ag_2S solid. Dried Ag_2S solids were reacted with F_2 (g) in a nickel bomb at 250 ˚C for >12 hours to generate SF_6 gas, which was purified via gas chromatography and analyzed on a MAT-253 in dual inlet mode in the Stable Isotope Laboratory at McGill University (See Crockford et al., 2016 for complete methods). Isotope compositions are reported in classical δ notations. The $\delta^{18}O$ is relative to Vienna Standard Mean Ocean Water (VSMOW), with an analytical precision better than ±0.3‰. Triple sulfur isotope compositions are reported related to Vienna Canyon Diablo Troilite (VCDT). The analytical errors for $\delta^{34}S$ and $\Delta^{33}S$ are ±0.3‰ and ±0.01‰ respectively.

3. Results

Oxygen isotope and triple sulfur isotope compositions of barite samples are listed in Table 1. Data points can be interpreted as two distinct groups within $\delta^{18}O$-$\delta^{34}S$ space, with samples bearing $\delta^{34}S$ values of less than 52.9‰ and a $\delta^{18}O$-$\Delta\delta^{34}S$ slope of

177 0.38±0.03 (with 95% confidence interval, n=13) denoted as “Barite 1” and samples
178 with $\delta^{34}S$ values greater than 62.6‰ and a $\delta^{18}O$-$\Delta\delta^{34}S$ slope of 0.21±0.04 (n=4)
179 denoted “Barite 2” (Fig. 2). For Barite 1, the $\Delta^{33}S$ correlates negatively with $\delta'^{34}S$
180 values (R^2=0.75, N=13), however, the 4 data points of Barite 2 do not overlap with
181 the $\Delta^{33}S$-$\delta'^{34}S$ trend defined by Barite 1 (Fig. 3).
182
183 **4. Discussion**
184 To establish a $\Delta^{33}S$-$\delta'^{34}S$ relationship for a pore-water sulfate profile in a typical
185 SD-AOM-dominated modern sedimentary setting, we first demonstrate that the
186 collected barite samples from the five different sites in the Gulf of Mexico are a good
187 model-environment (4.1). Next, we construct a model to fit observed $\Delta^{33}S$-$\delta'^{34}S$ data
188 (4.2). A reaction-transport model provides us a $^{33}\theta$ value under certain assumptions
189 (4.3). Finally, derived $^{33}\theta$ values and $\Delta^{33}S$-$\delta'^{34}S$ relationships for an
190 SD-AOM-dominated sedimentary profile is then compared with those of
191 OSR-dominated ones (4.4).
192 *4.1 SD-AOM derived barite*
193 Cold-seep barite collected from the five sites in the Gulf of Mexico captured the
194 original isotope signals of pore-water sulfate in an SD-AOM-dominated setting. This
195 is evident from the isotopic trajectory of $\delta^{18}O$-$\delta^{34}S$ trends within barite samples (Fig.
196 2). Both the oxygen and sulfur isotope compositions of sulfate are affected by kinetic
197 isotope fractionations associated with individual enzymatic reactions as well as
198 material transport. Specifically, sulfate $\delta^{18}O$ is also influenced by equilibrium

partitioning between intracellular water and intermediate valence state sulfur species (e.g., Brunner et al., 2005; Wortmann et al., 2007). The disparity in the behaviors of sulfur and oxygen isotope fractionations has made it possible to distinguish different electron donors by examining the slope of $\delta^{18}O$-$\delta^{34}S$ trajectories for residual sulfate pools (Antler et al., 2014, 2015; Feng et al., 2016). In OSR-dominated sediments, the back flux of intracellular intermediate valence state sulfur species to sulfate is apparently larger than in other sulfate reduction processes, which has been suggested to be due to the limitation of electron donors (e.g., Antler et al., 2013). Such conditions would cause the residual sulfate $\delta^{18}O$ value to increase faster than its corresponding $\delta^{34}S$ value and therefore lead to an apparent slope or a $\Delta\delta^{18}O/\Delta\delta^{34}S$ ratio greater than 0.7, as has been confirmed in marine sediments (e.g. Antler et al., 2014). Conversely, in SD-AOM dominated environments, a higher rate of sulfate reduction allows for a smaller back flux of intracellular intermediate valence state sulfur species and therefore leads to a lower $\Delta\delta^{18}O/\Delta\delta^{34}S$ ratio (0.24-0.5) in pore-water sulfate profiles (Brunner et al., 2005; Antler et al., 2013). Therefore, the low $\delta^{18}O$-$\delta^{34}S$ slopes (0.38 and 0.21) displayed in Fig. 2 are consistent with these cold-seep barites being precipitated in an SD-AOM-dominated environment. The inference that this is indeed an SD-AOM-dominated environment is also evident from observed $\delta^{13}C$ values (as low as -46.4‰) of the seep carbonate minerals associated within the barite samples from these sites (Feng and Roberts, 2011). The four data of group Barite 2, with $\delta^{34}S > 62.6$‰ and $\delta^{18}O > 22.6$‰, have a shallower slope (Fig. 2). This shift can be explained by two non-mutually exclusive processes: 1) the residual

sulfate $\delta^{18}O$ was approaching an apparent oxygen isotope equilibrium value that is set by the seawater $\delta^{18}O$ value, while reversibility of the whole microbial S-cycling processes did not change; and 2) the reversibility of the whole microbial S-cycling processes has changed to a different mode due to low sulfate concentrations.

4.2 Application of a reaction-transport model

A realistic physical model is critical to correctly deduce diagnostic α values and therefore a $^{33}\theta$ value of a triple sulfur isotope system. Due to the inevitable diffusion and advection mixing effects on sulfate isotope ratios in natural environments, a reaction-transport model should be applied. A Rayleigh model has previously been used to explain the observed linear correlations of $\delta^{18}O$ and $\delta^{34}S$ values in SD-AOM dominated environments (Antler et al., 2015). However, studies (e.g., Aharon and Fu, 2003; Druhan and Maher 2017) have demonstrated that the diagnostic α for the system would is underestimated when a Rayleigh model is applied to fit sulfate concentrations and isotope compositions in a pore-water profiles.

Here, we developed a 1-D diagenetic reaction-transport model to fit the linear correlation of $\Delta^{33}S$ vs. $\delta'^{34}S$ to calculate the diagnostic α. Our model has a set of assumptions: 1) We regard the data from the 5 different cold-seep sites as representative of steady-state pore-water sulfate at different depths of one pore-water profile; 2) The $^{34}\alpha$ and $^{33}\alpha$ of SD-AOM processes are constant among samples in group Barite 1. Wing and Halevy (2014) also suggested that the $1000\ln^{34}\alpha$ value is only weakly sensitive to external sulfate concentrations, and is insensitive to sulfide concentrations under high cell-specific sulfate reduction rates (csSRR); 3) The 1000ln

243 $^{34}\alpha$ values range from -30‰ to -10‰ more positive than in OSR-dominated sediments
244 (Deusner et al., 2014; Sivan et al., 2014); 4) Both diffusion and advection play critical
245 roles in mass transfer; 5) There is no isotope fractionation during sulfate diffusion
246 within pore waters (Wortmann and Chernyavsky 2011); 6) Sulfate reduction rates in
247 pore-waters is a first-order reaction with respect to sulfate concentration. In an earlier
248 study (Berner, 1964), sulfate reduction is treated as a first-order reaction with respect
249 to the content of "utilizable organic matter". That is indeed the case in typical marine
250 sediments where "utilizable organic matter" is limited. In the studied cold seep
251 environments, however, the concentration of methane in subsurface sediments is high,
252 thus, is not the limiting component during sulfate-derived methane oxidation. This is
253 supported by the observed widespread occurrence of gas hydrates in the shallow
254 subsurface (less than 6m) of the Gulf of Mexico (e.g., Sassen et al., 1999) and a
255 measured low $\Delta\delta^{18}O/\Delta\delta^{34}S$ ratio in sulfate (Antler et al., 2015; Feng et al., 2016;
256 Antler and Pellerin, 2018). Therefore, in our studied cold-seep system, the rate of
257 sulfate reduction is limited by sulfate concentration.

258 With these conditions, steady-state mass conservation for sulfate can be
259 described by the equation below (Berner 1964):

260 $$D\frac{\partial^2 C}{\partial Z^2} - \omega\frac{\partial C}{\partial Z} - kC = 0 \quad (1)$$

261 where D is the diffusion coefficient of sulfate in the sediment pore-water, C is the
262 pore water sulfate concentration, Z is the depth, k is the reaction rate constant of
263 sulfate reduction; velocity of advection ω is a sum of the externally imposed flow
264 velocity and the upward directed velocity caused by compaction. With the boundary

conditions of C=C_0 for Z=0 and C=0 for Z at infinity, Eq. (1) can be solved as:

$$C = C_0 EXP(\frac{\omega - \sqrt{\omega^2 + 4Dk}}{2D} * Z) \quad (2)$$

Similarly, the concentrations of different sulfate isotopologues ($^{32}SO_4^{2-}$, $^{33}SO_4^{2-}$, and $^{34}SO_4^{2-}$) can be calculated by Eq. (2). In δ′ notation, Eq. (2) can be reorganized as:

$$\delta'^{3i} S - \delta'^{3i} S_0 = (\frac{1 - \sqrt{1 + {}^{3i}\alpha^{32} k\phi}}{1 - \sqrt{1 + {}^{32} k\phi}} - 1) \ln f \quad (3)$$

where $^{3i}\alpha$=^{3i}k/^{32}k, 3i=33 or 34, Φ is equal to $4D/\omega^2$, $\delta'^{3i}S_0$ is the $\delta'^{3i}S$ value at Z=0, and f is the ratio of $^{32}C/^{32}C_0$. Since the isotope fractionation associated with sulfate diffusion is assumed to be 1, $\Delta^{33}S$ values can be calculated by,

$$\frac{\Delta^{33} S - \Delta^{33} S_0}{\delta'^{34} S - \delta'^{34} S_0} = \frac{\sqrt{1 + {}^{32} k\phi} - \sqrt{1 + {}^{33}\alpha^{32} k\phi}}{\sqrt{1 + {}^{32} k\phi} - \sqrt{1 + {}^{34}\alpha^{32} k\phi}} - 0.515 \quad (4)$$

where $\Delta^{33}S_0$ is the $\Delta^{33}S$ value at Z=0. Equation (4) shows that $\Delta^{33}S$ values are linearly correlated with $\delta'^{34}S$ values, and the slope is determined by α, k, and Φ.

We should note that the linear relationship between the $\Delta^{33}S$ and $\delta'^{34}S$ values is deduced for sulfate from different depths at one vertical pore-water profile. However, our samples presented here are from different sites. Therefore, the linear relationship between $\Delta^{33}S$ and $\delta'^{34}S$ values for these samples is not expected if the $\Delta^{33}S_0$, $\delta'^{34}S_0$, α, k, and Φ differ greatly among these sites. For example, different $\Delta^{33}S_0$ and $\delta'^{34}S_0$ values for these sites will result in parallel lines given the same α, k, and Φ, while different α, k, and Φ values will lead to a poor linear correlation between $\Delta^{33}S$ and $\delta'^{34}S$ values given the same $\Delta^{33}S_0$ and $\delta'^{34}S_0$. In contrast, our results (Fig. 3) show that barite samples from these 5 different sites form a good linear correlation between $\Delta^{33}S$ and $\delta'^{34}S$ values, and the modern value of seawater sulfate plots along the

extension of the line defining this linear correlation in Fig. 3 within errors. This result indicates that these different sites share similar $\Delta^{33}S$-$\delta'^{34}S$ slopes as well as $\Delta^{33}S_0$ and $\delta'^{34}S_0$ values (i.e., the isotope composition of seawater sulfate), which validates one of our initial assumptions.

4.3 $^{33}\theta$ value for SD-AOM processes

As shown in Eq. (4), the $\Delta^{33}S$-$\delta'^{34}S$ is determined by α, k, D, and ω. Therefore, $^{33}\theta$ values can be constrained by the determined $\Delta^{33}S$-$\delta'^{34}S$ slope if k, D, and ω can be constrained independently. While it is impossible to constrain k, D, and ω by our current measurements, we found that a smaller ω requires a larger $^{33}\theta$ to reproduce the observed $\Delta^{33}S$-$\delta'^{34}S$ slope (Table 2). In other words, when ω=0, i.e. without advection, Equation (4) will give the upper $^{33}\theta$ limit of SD-AOM processes. We also found that this upper-limit $^{33}\theta$ value is near the real $^{33}\theta$ value after we tested for ω values that are smaller than 60 cm/yr, which is a reasonable advection rate for cold-seep area (Lapham et al., 2008) (Table 2). Therefore, it is reasonable to assume that ω=0 when constraining $^{33}\theta$. At ω=0, the slope of $\Delta^{33}S/\delta'^{34}S$ will be determined by:

$$\frac{\Delta^{33}S-\Delta^{33}S_0}{\delta'^{34}S-\delta'^{34}S_0}=\frac{\sqrt{^{33}\alpha}-1}{\sqrt{^{34}\alpha}-1}-0.515 \quad (5)$$

Therefore, the $^{33}\theta$ for SD-AOM can be obtained by the observed slope of $\Delta^{33}S$-$\delta'^{34}S$ at a given $^{34}\alpha$ value.

Eq. (5) shows that $^{33}\theta$ is dependent upon $^{34}\alpha$. The $1000\ln^{34}\alpha$ reported for microbial dissimilatory sulfate reduction has a broad range and can be as low as -70‰ (e.g., Sim et al., 2011a). Typically, $1000\ln^{34}\alpha$ is more negative than -40‰ in an OSR-dominated marine pore-water profile (e.g., Claypool et al., 2004), and more

positive than -40‰ in an SD-AOM-dominated one (Aharon and Fu, 2000; Deusner et al., 2014; Sivan et al., 2014). Numerous studies have demonstrated that the expressed sulfur isotope fractionation associated with microbial dissimilatory sulfate reduction decrease with an increasing csSRR and eventually the $1000\ln^{34}\alpha$ will reach a high, constant, value at -10‰ to -30‰ (e.g., Leavitt et al., 2013; Deusner et al., 2014). Therefore, a value ranging from -40‰ to -10‰ should be reasonable for $1000\ln^{34}\alpha$ associated with SD-AOM where sulfate reduction rates are relatively high, e.g. 600 times higher than in methane-limited sediments (Aharon and Fu, 2000). However, if we consider $1000\ln^{34}\alpha$ values at -40‰ to -30‰, Equation (5) would give pairs of $^{33}\theta$ and $1000\ln^{34}\alpha$ values that are outside of the $^{33}\theta$-$1000\ln^{34}\alpha$ field obtained from culture experiments (Fig. 4) and outside of the prediction given by a kinetic model (Wing and Halevy, 2014). Therefore, the range of $1000\ln^{34}\alpha$ can be further constrained to be between -30‰ to -10‰ for our Barite 1 samples. At these $^{34}\alpha$ ranges, the $^{33}\theta$ is calculated to range from 0.5100 to 0.5112 (±0.0005) using group Barite 1 data (Fig. 4).

The terminal electron acceptor (sulfate) concentration also plays a role in determining the magnitude of sulfur isotope fractionation associated with SD-AOM (e.g., Habicht et al., 2005; Deusner et al., 2014). This raises the question as to whether sulfate concentrations influence $^{33}\theta$ values during SD-AOM. Wing and Halevy (2014) suggested that moderate to high csSRR would lead to a less negative $1000\ln^{34}\alpha$, which is only weakly sensitive to external sulfate concentrations. The sulfate reduction rate is generally high in methane-rich environments. Therefore, both

330 $1000\ln^{34}\alpha$ and $^{33}\theta$ values should be insensitive to sulfate concentration changes during
331 the formation of group Barite 1, which is supported by linear $\Delta^{33}S$-$\delta'^{34}S$ and $\delta^{18}O$-$\delta^{34}S$
332 correlations (Figs. 2 and 3). In contrast to results from Barite 1, during the
333 precipitation of group Barite 2 ($\delta^{34}S$ > 62.7‰), the corresponding sulfate
334 concentration must have been very low. In the absence of *k* and ω values, we could
335 not speculate on the sulfate concentration during the precipitation of group Barite 2.
336 Here if ω is assumed to be 0, and C_0 and $\delta^{34}S_0$ is assumed to be 28 mM and 21‰
337 respectively, the corresponding sulfate concentration would be at 1.8 mM to 6.8 μM
338 for a given $1000\ln^{34}\alpha$ values of -30‰ to -10‰ (calculated with Eq. 3). Under such
339 low sulfate concentrations, high internal sulfide concentrations would increase the
340 reversibility in the APS reduction step (Wing and Halevy 2014). Consequently,
341 diagnostic $^{33}\theta$ and $1000\ln^{34}\alpha$ of SD-AOM would have changed, which can explain the
342 deviation in the data plot of group Barite 2 from that of group Barite 1 (Fig. 3). A high
343 degree of reversibility in the APS reduction step would lead $\delta^{18}O$ values to reach an
344 apparent equilibrium between sulfate and pore-waters, and a shallower slope along a
345 $\delta^{18}O$-$\delta^{34}S$ trajectory as observed in Fig. 2. At low sulfate concentrations, the isotope
346 fractionations of SD-AOM are poorly constrained in our model due to a limited
347 availability of data. Overall, the diagnostic $^{33}\theta$ values (0.5100-0.5112) with $1000\ln^{34}\alpha$
348 values between -30‰ and -10‰ reflect high csSRR in the studied
349 SD-AOM-dominated setting where sulfate concentrations are likely to be much
350 higher than 1.8 mM.

351 The observed apparent differences between $^{33}\theta$ values or $^{33}\theta$-$1000\ln^{34}\alpha$

352 trajectories between SD-AOM and OSR processes is most likely a manifestation of
353 the difference in reversibility of a set of enzyme or non-enzyme-catalyzed reactions.
354 Biochemical reversibility plays a critical role in sulfate reduction (Wing and Halevy,
355 2014) and the reversibility is determined by the electron transfer efficiency from
356 electron donor to sulfate reduction pathway. The typically high sulfate reduction rate
357 associated with AOM indicates a high electron transfer efficiency from methane to
358 sulfate, which limits the reversibility of sulfate reduction reactions and results in less
359 negative $1000\ln^{34}\alpha$ and smaller $^{33}\theta$ values. If organic molecules (e.g. ethanol, lactate,
360 glycerol) used in culture experiments (Sim et al., 2011b; Leavitt et al., 2013), can also
361 transfer their electrons to the sulfate reduction pathway efficiently, similarly less
362 negative $1000\ln^{34}\alpha$ and smaller $^{33}\theta$ values would be achieved. This is a possible
363 reason why our obtained $^{33}\theta$-$1000\ln^{34}\alpha$ range associated with SD-AOM overlaps with
364 the $^{33}\theta$-$1000\ln^{34}\alpha$ range reported in culture experiments (Fig. 4). However, the organic
365 matter in typical marine sediments is quite recalcitrant and difficult to be utilized by
366 sulfate-reducing bacteria (Berner, 1964), which limits the electron transfer efficiency.
367 This is a possible reason as to why more negative $1000\ln^{34}\alpha$ values were observed for
368 sulfate reduction in typical marine sediments. Note that a high net sulfate reduction
369 rate does not necessarily correspond to a high electron transfer efficiency, e.g., as
370 reported in organic rich sediments (Masterson et al., 2018).

371 *4.4 Dynamics of $\Delta^{33}S$ vs. $\delta'^{34}S$ in different marine settings*

372 Currently, triple-sulfur isotope data associated with microbial dissimilatory
373 sulfate reduction in modern marine sediments are limited. Our observed $\Delta^{33}S$-$\delta'^{34}S$

correlation among the cold-seep barite samples is negative. However, reported $\Delta^{33}S$-$\delta'^{34}S$ correlations have typically been positive for pore-water sulfate profiles in OSR-dominated environments (Fig. 5) (e.g., Strauss et al., 2012; Pellerin et al., 2015; Masterson et al., 2018). The reason for these positive correlations in OSR-dominated environments is further explored here. First, the $1000\ln^{34}\alpha$ is more negative and $^{33}\theta$ value is higher in OSR-dominated settings. The typical $1000\ln^{34}\alpha$ value associated with OSR is usually more negative than -40‰ in marine sediments (e.g., Claypool et al., 2004) and the $^{33}\theta$ value ranges from 0.5125 to 0.5148 (e.g., Leavitt et al., 2013; Tostevin et al., 2014). Such ranges of $^{33}\theta$ and $1000\ln^{34}\alpha$ values can only be defined through a positive $\Delta^{33}S$-$\delta'^{34}S$ correlation according to our reaction-transport model. Secondly, the reoxidative sulfur cycle coupled with disproportionation reactions can lead to higher $\Delta^{33}S$-$\delta'^{34}S$ slope in pore-water sulfate profiles. When sulfide oxidation occurs following disproportionation, the $\Delta^{33}S$-$\delta'^{34}S$ trajectory depends on the net sulfate removal rate instead of just the OSR rate. Both the $^{33}\theta$ and the degree of sulfur isotope fractionation of net sulfate removal increases with an increasing amount of sulfide reoxidation (Pellerin et al., 2015). For these reasons, we now have two contrasting $\Delta^{33}S$-$\delta'^{34}S$ correlations for residual sulfate between SD-AOM- and OSR-dominated settings. Therefore, we can potentially use triple sulfur isotope relationships ($\Delta^{33}S$-$\delta'^{34}S$) preserved in residual sulfate preserved in sedimentary rocks to distinguish these two sulfate reduction environments. This fossil residual sulfate can either be barite or carbonate-associated sulfate preserved in carbonates.

Disseminated pyrite grains are more commonly preserved than pore-water sulfate

within sedimentary records. If barite samples capture various stages of the sulfate reservoir in pore-waters from SD-AOM settings and display a distinctly negative $\Delta^{33}S$-$\delta'^{34}S$ correlation, the corresponding product HS^- or H_2S could also display a similar negative $\Delta^{33}S$-$\delta'^{34}S$ correlation. A condition for this to occur is to have sufficient Fe (II) in the system to react with the reduced S as FeS and eventually as FeS_2. In an OSR-dominated sediment, a positive $\Delta^{33}S$-$\delta'^{34}S$ correlation for pore-water sulfate profiles may not be preserved among disseminated pyrite grains because pyrite grains tend to represent integrated signatures instead of a set of snap-shots of product HS^- or H_2S in an SD-AOM-dominated profile. Further work on the triple sulfur isotope composition of pyrite and H_2S in modern SD-AOM-dominated environments is needed before we can apply these new findings to the sedimentary record.

5. Conclusion

Barite samples collected in five cold-seep sites in the Gulf of Mexico represent various snapshots of residual sulfate in pore-water, as evident from a low $\delta^{18}O$-$\delta^{34}S$ slope (0.38) among these samples. These cold-seep barites further exhibit a linear negative correlation in $\Delta^{33}S$-$\delta'^{34}S$ space. Applying a reaction-transport model, we obtained a diagnostic $^{33}\theta$ value with the upper limit ranging from 0.5100 to 0.5112 (±0.0005) assuming a $1000\ln^{34}\alpha$ (sulfide-sulfate) value from -30‰ to -10‰ for SD-AOM in these SD-AOM-dominated environments. This $^{33}\theta$ value is lower than that of typical OSR processes in marine environments where $1000\ln^{34}\alpha$ is typically more negative than that of SD-AOM processes. Furthermore, barite samples from

SD-AOM-dominated environments display a negative $\Delta^{33}S$-$\delta'^{34}S$ correlation, which is in direct contrast to the positive correlations commonly observed for pore-water sulfate profiles from OSR-dominated settings. The diagnostically low $^{33}\theta$ parameter and the negative $\Delta^{33}S$-$\delta'^{34}S$ correlation can be preserved in barite, carbonate associated sulfates, and perhaps among disseminated pyrite grains in the sedimentary record, providing potential for an independent marker for SD-AOM throughout the past 2.4 billion years of Earth history.

Acknowledgment

Barite samples from the Gulf of Mexico were collected on projects funded by the Bureau of Ocean Energy Management and NOAA's National Undersea Research Program. We thank H.H. Roberts for providing the samples. Funding was provided by the NSF of China (Grants: 41773091, 4176113408, 41730528 and 41490635). Financial support is partially provided by the strategic priority research program (B) of CAS (XDB18010104) to HB. PWC acknowledges funding from the Agouron Institute. We thank two anonymous reviewers for their constructive comments.

Reference

Aharon P., 1991. Chronostratigraphy and bathymetry models of the last sea level cycle from paired plankton/benthic foraminifera stable isotopes in the Gulf of Mexico slope sediments. Unpublished report, Exxon Co., USA, p. 150.

Aharon, P., Fu, B.S., 2000. Microbial sulfate reduction rates and sulfur and oxygen

isotope fractionations at oil and gas seeps in deepwater Gulf of Mexico. Geochim. Cosmochim. Acta 64, 233-246.

Aharon, P., Fu, B.S., 2003. Sulfur and oxygen isotopes of coeval sulfate-sulfide in pore fluids of cold seep sediments with sharp redox gradients. Chem. Geol. 195, 201-218.

Antler G., Turchyn A. V., Ono S., Sivan O. and Boask T. 2017. Combined ^{34}S, ^{33}S and ^{18}O isotope fractionations record different intracellular steps of microbial sulfate reduction. Geochim. Cosmochim. Acta 203, 364–380.

Antler, G., Pellerin, A., 2018. A Critical Look at the Combined Use of Sulfur and Oxygen Isotopes to Study Microbial Metabolisms in Methane-Rich Environments. Front. Microbiol. 9, 519.

Antler, G., Turchyn, A.V., Herut, B., Davies, A., Rennie, V.C.F., Sivan, O., 2014. Sulfur and oxygen isotope tracing of sulfate driven anaerobic methane oxidation in estuarine sediments. Estuar. Coast. Shelf Sci. 142, 4-11.

Antler, G., Turchyn, A.V., Herut, B., Sivan, O., 2015. A unique isotopic fingerprint of sulfate-driven anaerobic oxidation of methane. Geology 43, 619-622.

Antler, G., Turchyn, A.V., Rennie, V., Herut, B., Sivan, O., 2013. Coupled sulfur and oxygen isotope insight into bacterial sulfate reduction in the natural environment. Geochim. Cosmochim. Acta 118, 98-117.

Bao, H.M., 2006. Purifying barite for oxygen isotope measurement by dissolution and reprecipitation in a chelating solution. Anal. Chem. 78, 304-309.

Berner, R.A., 1964. An Idealized Model of Dissolved Sulfate Distribution in Recent

462 Sediments. Geochim. Cosmochim. Acta 28, 1497-1503.
463 Bradley, A.S., Leavitt, W.D., Schmidt, M., Knoll, A.H., Girguis, P.R., Johnston, D.T.,
464 2016. Patterns of sulfur isotope fractionation during microbial sulfate reduction.
465 Geobiology 14, 91-101.
466 Bristow, T.F., Grotzinger, J.P., 2013. Sulfate availability and the geological record of
467 cold-seep deposits. Geology 41, 811-814.
468 Brunner, B., Bernasconi, S.M., Kleikemper, J., Schroth, M.H., 2005. A model for
469 oxygen and sulfur isotope fractionation in sulfate during bacterial sulfate
470 reduction processes. Geochim. Cosmochim. Acta 69, 4773-4785.
471 Campbell, K.A., 2006. Hydrocarbon seep and hydrothermal vent paleoenvironments
472 and paleontology: Past developments and future research directions. Palaeogeogr.
473 Palaeoclimatol. Palaeoecol. 232, 362-407.
474 Claypool G. E., 2004. Ventilation of marine sediments indicated by depth profiles of
475 pore water sulfate and δ^{34}S. Spec. Publ. Geochem. Soc. 9, 59-65.
476 Claypool G.E., Holser W.T., Kaplan I.R., Sakai H. and Zak I., 1980. The age curves
477 of sulfur and oxygen isotopes in marine sulfate and their mutual interpretation.
478 Chemical. Geol. 28, 199- 260
479 Crockford, P.W., Cowie, B.R., Johnston, D.T., Hoffman, P.F., Sugiyama, I., Pellerin,
480 A., Bui, T.H., Hayles, J., Halverson, G.P., Macdonald, F.A., Wing, B.A., 2016.
481 Triple oxygen and multiple sulfur isotope constraints on the evolution of the
482 post-Marinoan sulfur cycle. Earth Planet. Sci. Lett. 435, 74-83.
483 Deusner, C., Holler, T., Arnold, G.L., Bernasconi, S.M., Formolo, M.J., Brunner, B.,

2014. Sulfur and oxygen isotope fractionation during sulfate reduction coupled to anaerobic oxidation of methane is dependent on methane concentration. Earth Planet. Sci. Lett. 399, 61-73.

Deusner, C., Holler, T., Arnold, G.L., Bernasconi, S.M., Formolo, M.J., Brunner, B., 2014. Sulfur and oxygen isotope fractionation during sulfate reduction coupled to anaerobic oxidation of methane is dependent on methane concentration. Earth Planet. Sci. Lett. 399, 61-73.

Druhan, J.L., Maher, K., 2017. The influence of mixing on stable isotope ratios in porous media: A revised Rayleigh model. Water Resour. Res. 53, 1101-1124.

Egger, M., Riedinger, N., Mogollon, J.M., Jørgensen, B.B., 2018. Global diffusive fluxes of methane in marine sediments. Nat. Geosci. 11, 421-425.

Feng, D., Peng, Y.B., Bao, H.M., Peckmann, J., Roberts, H.H., Chen, D.F., 2016. A carbonate-based proxy for sulfate-driven anaerobic oxidation of methane. Geology 44, 999-1002.

Feng, D., Roberts, H.H., 2011. Geochemical characteristics of the barite deposits at cold seeps from the northern Gulf of Mexico continental slope. Earth Planet. Sci. Lett. 309, 89-99.

Girguis, P.R., Orphan, V.J., Hallam, S.J., DeLong, E.F., 2003. Growth and methane oxidation rates of anaerobic methanotrophic archaea in a continuous-flow bioreactor. Appl. Environ. Microb. 69, 5472-5482.

Fichtner, V., Strauss, H., Immenhauser, A., Buhl, D., Neuser, R.D., Niedermayr, A., 2017. Diagenesis of carbonate associated sulfate. Chem. Geol. 463, 61-75.

506 Habicht, K.S., Salling, L.L., Thamdrup, B., Canfield, D.E., 2005. Effect of low sulfate
507 concentrations on lactate oxidation and isotope Fractionation during sulfate
508 reduction by Archaeoglobus fulgidus strain Z. Appl. Environ. Microb. 71,
509 3770-3777.
510 Holler, T., Wegener, G., Niemann, H., Deusner, C., Ferdelman, T.G., Boetius, A.,
511 Brunner, B., Widdel, F., 2011. Carbon and sulfur back flux during anaerobic
512 microbial oxidation of methane and coupled sulfate reduction. Proc. Natl. Acad.
513 Sci. 108, E1484-E1490.
514 Joye, S.B., Boetius, A., Orcutt, B.N., Montoya, J.P., Schulz, H.N., Erickson, M.J.,
515 Lugo, S.K., 2004. The anaerobic oxidation of methane and sulfate reduction in
516 sediments from Gulf of Mexico cold seeps. Chem. Geol. 205, 219-238.
517 Kaim, A., Jenkins, R.G., Tanabe, K., and Kiel, S., 2014, Mollusks from late Mesozoic
518 seep deposits, chiefly in California: Zootaxa, v. 3861, p. 401–440.
519 Lapham, L.L., Alperin, M., Chanton, J., Martens, C., 2008. Upward advection rates
520 and methane fluxes, oxidation, and sources at two Gulf of Mexico brine seeps.
521 Mar. Chem. 112, 65-71.
522 Leavitt, W.D., Halevy, I., Bradley, A.S., Johnston, D.T., 2013. Influence of sulfate
523 reduction rates on the Phanerozoic sulfur isotope record. Proc. Natl. Acad. Sci.
524 110, 11244-11249.
525 Lin, Z.Y., Sun, X.M., Strauss, H., Lu, Y., Gong, J.L., Xu, L., Lu, H.F, Teichert,
526 B.M.A., Peckmann, J., 2017. Multiple sulfur isotope constraints on
527 sulfate-driven anaerobic oxidation of methane: Evidence from authigenic pyrite

528 in seepage areas of the South China Sea. Geochim. Cosmochim. Acta 211,
529 153-173.
530 Masterson A.L., 2016. Multiple Sulfur Isotope Applications in Diagenetic Models and
531 Geochemical Proxy Records. Doctoral dissertation, Harvard University,
532 Graduate School of Arts & Sciences.
533 Masterson, A., Alperin M.J., Berelson, W.M., Johnston, D.T., 2018. Interpreting
534 multiple sulfur isotope signals in modern anoxic sediments using a full
535 diagenetic model (California-Mexico margin: Alfonso Basin). Am. J. Sci. P.
536 459-490.
537 Olson, S.L., Reinhard, C.T., Lyons, T.W., 2016. Limited role for methane in the
538 mid-Proterozoic greenhouse. Proc. Natl. Acad. Sci. 113, 11447-11452.
539 Ono, S.H., Keller, N.S., Rouxel, O., Alt, J.C., 2012. Sulfur-33 constraints on the
540 origin of secondary pyrite in altered oceanic basement. Geochim. Cosmochim.
541 Acta 87, 323-340.
542 Peckmann, J., Thiel, V., 2004. Carbon cycling at ancient methane–seeps. Chem. Geol.
543 205, 443-467.
544 Pellerin, A., Bui, T.H., Rough, M., Mucci, A., Canfield, D.E., Wing, B.A., 2015.
545 Mass-dependent sulfur isotope fractionation during reoxidative sulfur cycling: A
546 case study from Mangrove Lake, Bermuda. Geochim. Cosmochim. Acta 149,
547 152-164.
548 Reeburgh, W.S., 2007. Oceanic methane biogeochemistry. Chem Rev 107, 486-513.
549 Sassen, R., Sweet, S.T., Milkov, A.V., DeFreitas, D.A., Salata, G.G., McDade, E.C.,

1999. Geology and geochemistry of gas hydrates, central Gulf of Mexico continental slope. Trans. Gulf Coast Assoc. Geol. Soc. 49, 462 – 468.

Sim, M.S., Bosak, T., Ono, S., 2011a. Large sulfur isotope fractionation does not require disproportionation. Science 333, 74-77.

Sim, M.S., Ono, S., Donovan, K., Templer, S.P., Bosak, T., 2011b. Effect of electron donors on the fractionation of sulfur isotopes by a marine Desulfovibrio sp. Geochim. Cosmochim. Acta 75, 4244-4259.

Sivan, O., Antler, G., Turchyn, A.V., Marlow, J.J., Orphan, V.J., 2014. Iron oxides stimulate sulfate-driven anaerobic methane oxidation in seeps. Proc. Natl. Acad. Sci. 111, E4139-E4147.

Strauss, H., Bast, R., Cording, A., Diekrup, D., Fugmann, A., Garbe-Schonberg, D., Lutter, A., Oeser, M., Rabe, K., Reinke, D., Teichert, B.M.A., Westernstroer, U., 2012. Sulphur diagenesis in the sediments of the Kiel Bight, SW Baltic Sea, as reflected by multiple stable sulphur isotopes. Isot Environ Healt S 48, 166-179.

Tostevin, R., Turchyn, A.V., Farquhar, J., Johnston, D.T., Eldridge, D.L., Bishop, J.K.B., McIlvin, M., 2014. Multiple sulfur isotope constraints on the modern sulfur cycle. Earth Planet. Sci. Lett. 396, 14-21.

Turchyn, A.V., Brüchert, V., Lyons, T.W., Engel, G.S., Balci, N., Schrag, D.P., Brunner, B., 2010. Kinetic oxygen isotope effects during dissimilatory sulfate reduction: A combined theoretical and experimental approach. Geochim. Cosmochim. Acta 74, 2011-2024.

Wing, B.A., Halevy, I., 2014. Intracellular metabolite levels shape sulfur isotope

572 fractionation during microbial sulfate respiration. Proc. Natl. Acad. Sci. 111,
573 18116-18125.
574 Wortmann, U.G., Chernyavsky, B., Bernasconi, S.M., Brunner, B., Bottcher, M.E.,
575 Swart, P.K., 2007. Oxygen isotope biogeochemistry of pore water sulfate in the
576 deep biosphere: Dominance of isotope exchange reactions with ambient water
577 during microbial sulfate reduction (ODP Site 1130). Geochim. Cosmochim. Acta
578 71, 4221-4232.
579 Wortmann, U.G., Chernyavsky, B.M., 2011. The significance of isotope specific
580 diffusion coefficients for reaction-transport models of sulfate reduction in marine
581 sediments. Geochim. Cosmochim. Acta 75, 3046-3056.
582 Wu, N., Farquhar, J., 2013. Metabolic rates and sulfur cycling in the geologic record.
583 Proc. Natl. Acad. Sci. 110, 11217-11218.
584 Zhou, C.M., Guan, C.G., Cui, H., Ouyang, Q., Wang, W., 2016. Methane-derived
585 authigenic carbonate from the lower Doushantuo Formation of South China:
586 Implications for seawater sulfate concentration and global carbon cycle in the
587 early Ediacaran ocean. Palaeogeogr. Palaeoclimatol. Palaeoecol. 461, 145-155.
588

589 **Table captions**

590 **Table 1.** Oxygen isotope and triple sulfur isotope compositions of cold seep barite
591 samples collected from sites of GC415, GC237, GB338, GB697 and MC709 in the
592 Gulf of Mexico.

593 **Table 2.** The $^{33}\theta_{modeled}$ value is predicted with a given $1000\ln^{34}\alpha$ and ω value to best fit
594 the data of group Barite 1. The $\Delta^{33}S$-$\delta'^{34}S$ slope (i.e. $\Delta\Delta^{33}S$-$\Delta\delta'^{34}S$) is reproduced by a
595 given set of $1000\ln^{34}\alpha$, $^{33}\theta$ and ω values. Distinctly high $\Delta\Delta^{33}S/\Delta\delta'^{34}S$ values
596 reproduced with ω >0.6m/yr are observed. The sensitivity test is based on the
597 assumptions that C_0 and $\delta^{34}S_0$ are 28 mM and 21‰, respectively; D is 0.01m^2/yr
598 (Berner, 1978); and the reaction rate constant ^{32}k is assumed to be 1mol/m^2/yr
599 (Aharon 1991). The modeled $^{32}SO_4^{2-}$ concentration profile (sulfate consumed within
600 0.5 meter below the seafloor) is reasonable for cold-seep settings in the Gulf of
601 Mexico (Aharon and Fu, 2000).

602

603 **Figure captions**

604 **Fig. 1.** Sampling locations in the Gulf of Mexico.

605 **Fig. 2.** The $\delta^{18}O$-$\delta^{34}S$ values of seep barite from modern sediments at five sites in the
606 Gulf of Mexico. Analytical error is smaller than the sizes of the plotted symbols.

607 **Fig. 3.** The $\Delta^{33}S$-$\delta'^{34}S$ values of seep barites from modern sediments at five sites in
608 the Gulf of Mexico. Analytical errors for $\delta'^{34}S$ values are smaller than the size of
609 the individual symbols. The black line indicates the linear fit for samples of group
610 Barite 1, which yields a $\Delta^{33}S$-$\delta'^{34}S$ slope value of 0.00314±0.00052. The area

611 within the dotted line corresponds to the 95% confidence interval of this fit.

612 **Fig. 4.** Comparison of the $1000\ln^{34}\alpha$-$^{33}\theta$ relationships for published data from
613 non-methane based pure culture experiments (circles and squares, Sim et al.,
614 2011b; Leavitt et al., 2013) with that calculated for SD-AOM represented by our
615 barite data from five cold-seep sites in the Gulf of Mexico (solid line). The
616 calculation was done using the measured barite $\delta'^{34}S$ and $\Delta^{33}S$ data via Eq. (5).
617 The error (2σ) of the calculated $^{33}\theta$ value is 0.0005 for each given $1000\ln^{34}\alpha$,
618 constrained by the Monte Carlo method considering errors for the obtained
619 $\Delta^{33}S$-$\delta'^{34}S$ slope (Fig. 3). The dash lines show that the calculated $^{33}\theta$ value ranges
620 from 0.5100 to 0.5112 when the corresponding $1000\ln^{34}\alpha$ value ranges from -30‰
621 to -10‰.

622 **Fig. 5.** Comparison of $\Delta^{33}S$-$\delta'^{34}S$ trajectories from various OSR-dominated
623 pore-water sulfate profiles (data collected from Strauss et al., 2012; Pellerin et al.,
624 2015; Masterson 2016; Lin et al., 2017; Masterson et al., 2018) with that of
625 cold-seep barites from the Gulf of Mexico.

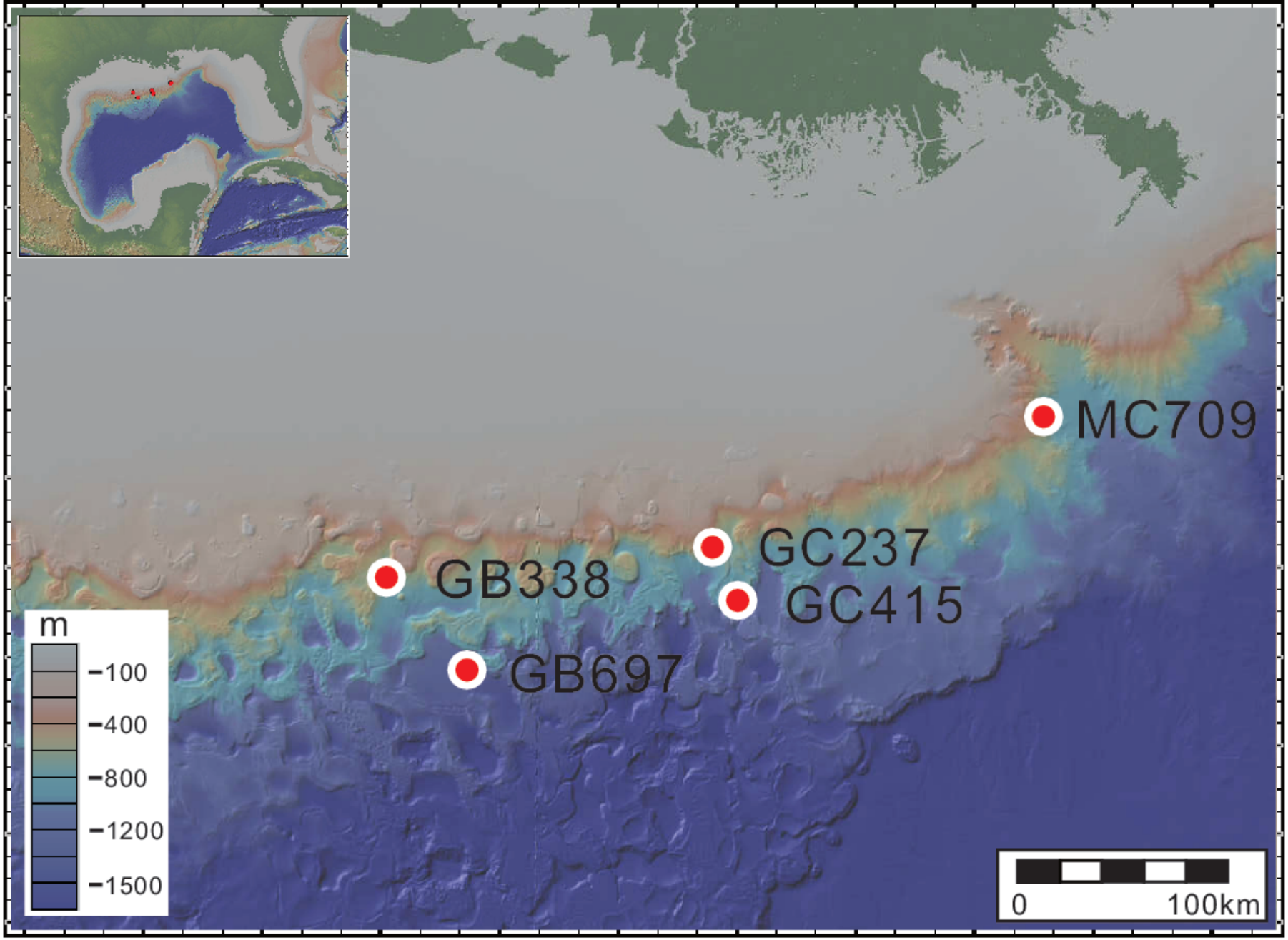
MC709
GC237
GC415
GB338
GB697
m
−100
−400
−800
−1200
−1500
0
100km
29°N
28°N
27°N
94°W
92°W
90°W

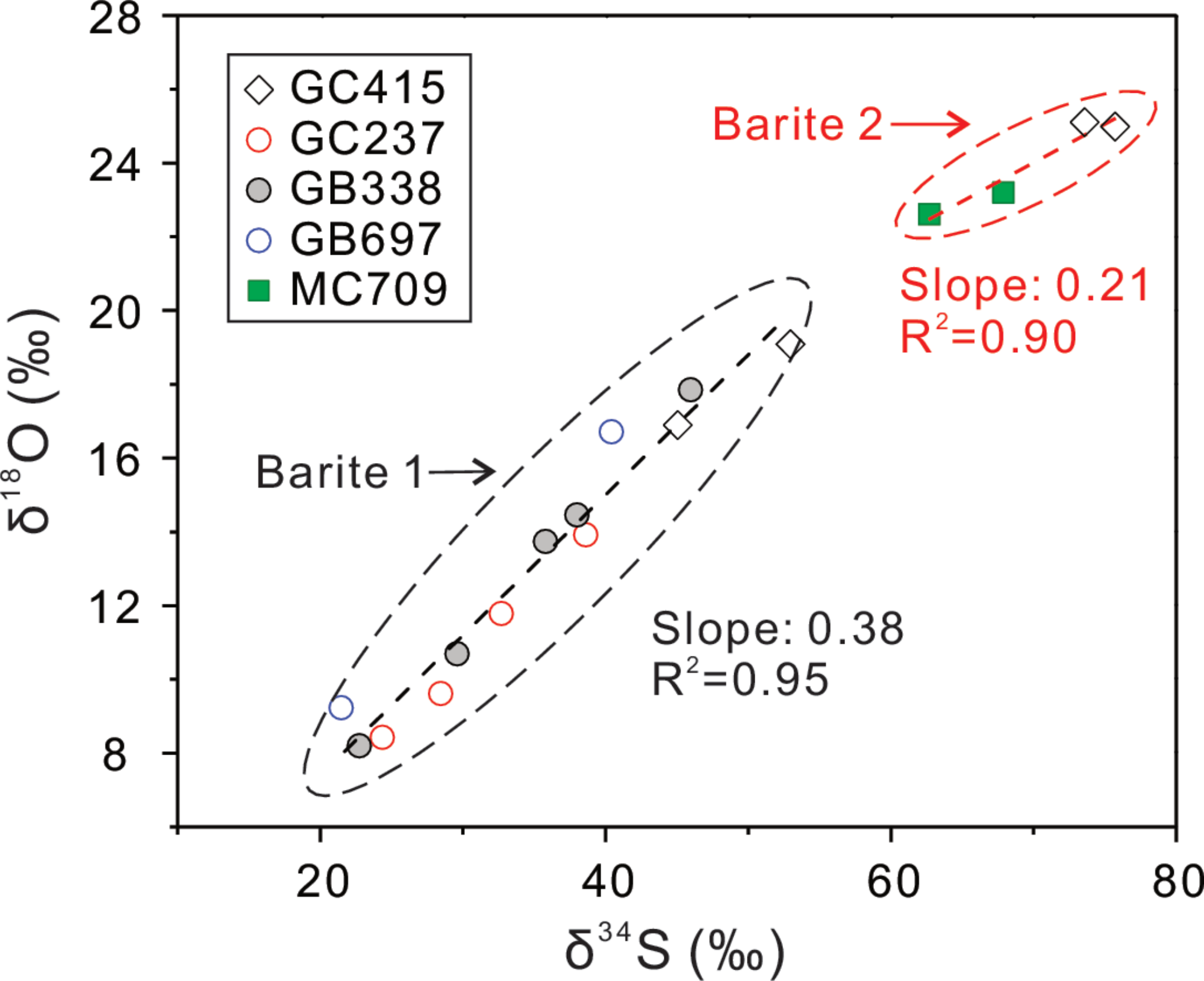
GC415
GC237
GB338
GB697
MC709
Barite 2
Slope: 0.21
R²=0.90
Barite 1
Slope: 0.38
R²=0.95
δ18O (‰)
δ34S (‰)
28
24
20
16
12
8
20
40
60
80

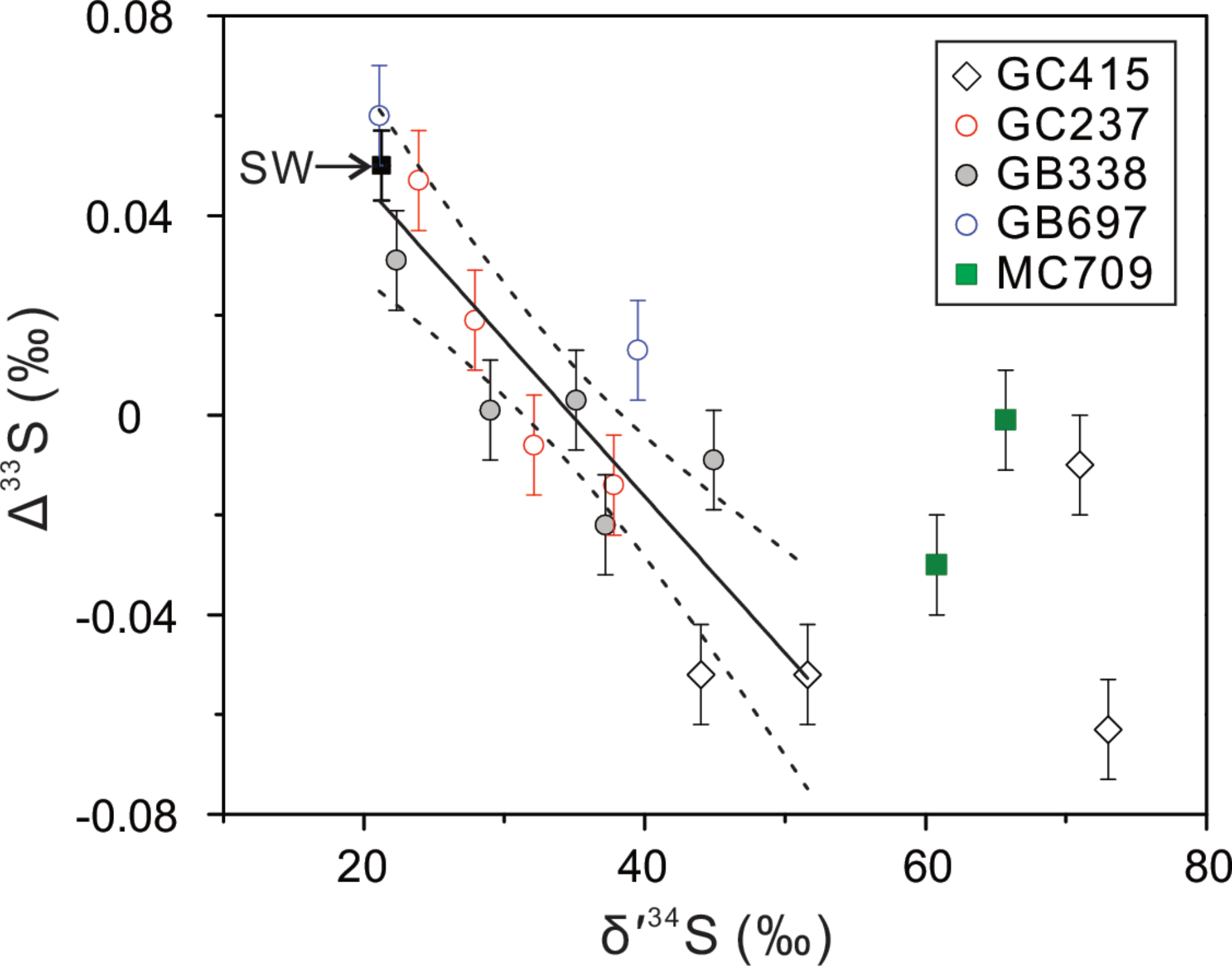
0.08
0.04
0
-0.04
-0.08
20
40
60
80
SW
GC415
GC237
GB338
GB697
MC709
Δ33S (‰)
δ′34S (‰)

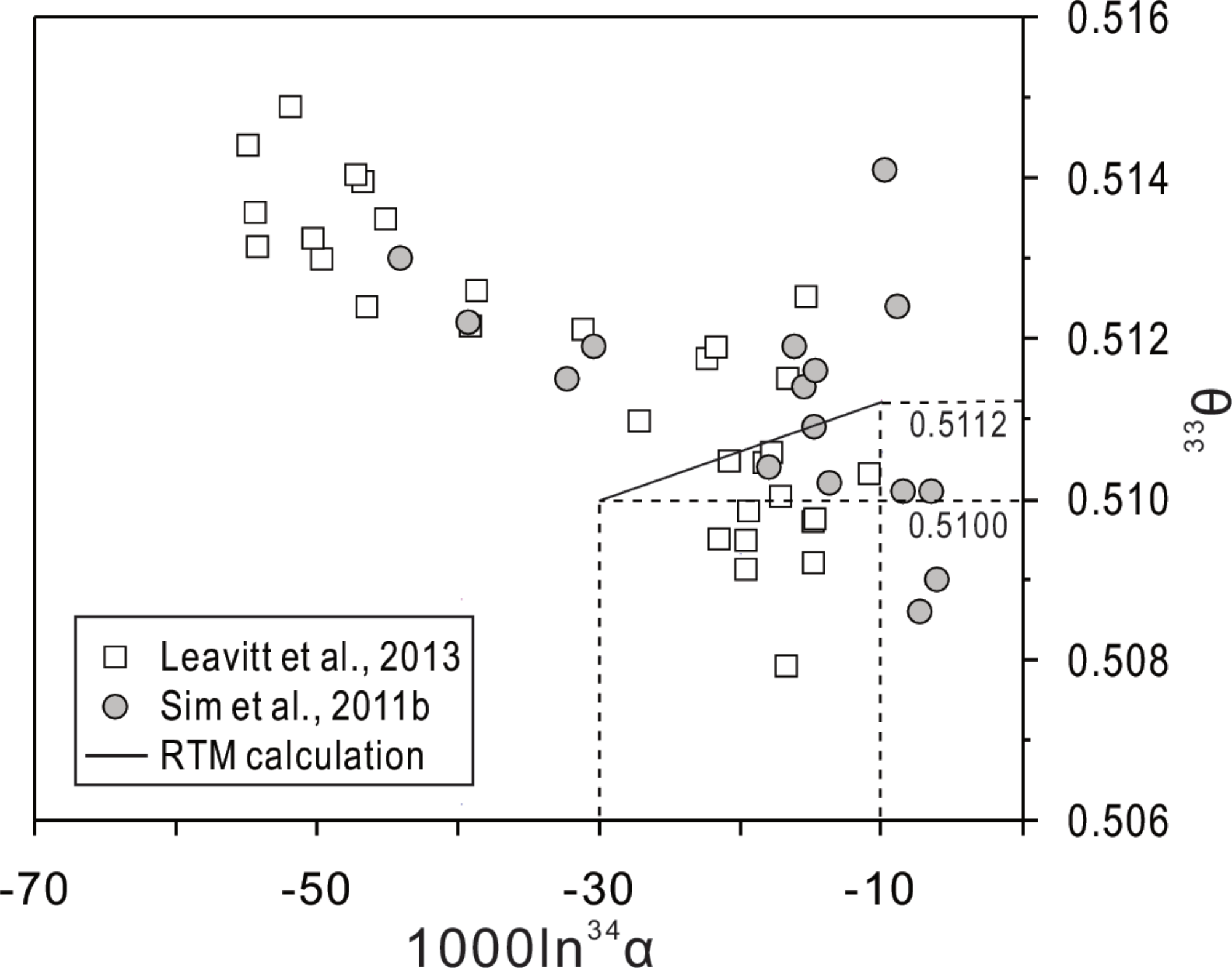
0.516
0.514
0.512
0.510
0.508
0.506
$^{33}\theta$
0.5112
0.5100
Leavitt et al., 2013
Sim et al., 2011b
RTM calculation
-70
-50
-30
-10
$1000\ln^{34}\alpha$

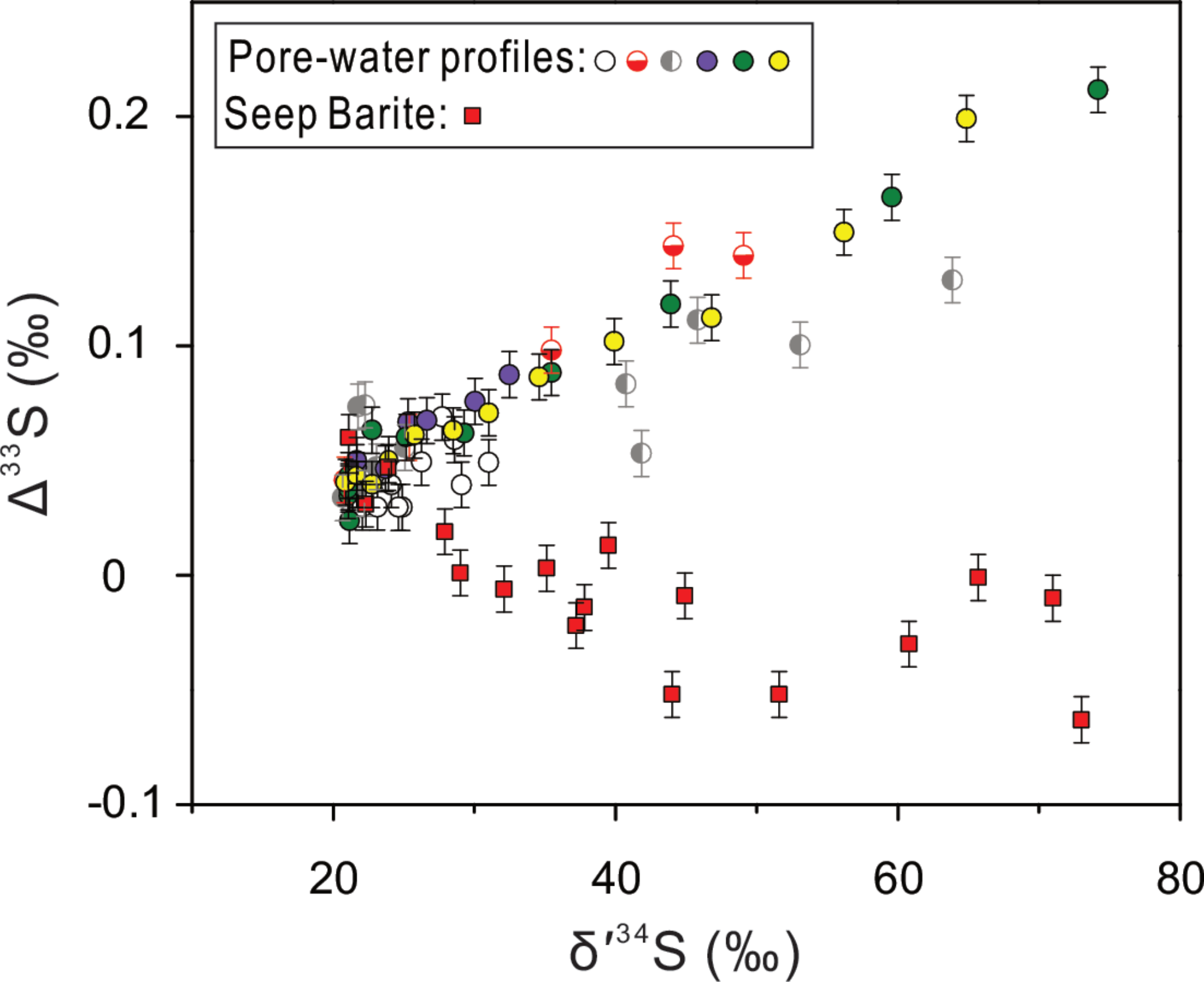
Pore-water profiles:
Seep Barite:
0.2
0.1
0
-0.1
$\Delta^{33}S$ (‰)
20
40
60
80
$\delta'^{34}S$ (‰)

Sites	Samples ID	$\delta^{18}O$ VSMOW	$\delta^{34}S$ VCDT	$\delta'^{34}S$ VCDT	$\Delta^{33}S$ VCDT
GC415	B1	25.0	75.7	73.0	-0.063
	B2	25.1	73.6	71.0	-0.010
	B3	19.1	52.9	51.6	-0.052
	B4	16.9	45.0	44.0	-0.052
GC237	B5	9.6	28.3	27.9	0.019
	B6	8.4	24.2	23.9	0.047
	B7	13.9	38.5	37.8	-0.014
	B8	11.8	32.6	32.1	-0.006
GB338	B9	13.7	35.7	35.1	0.003
	B10	17.8	45.9	44.9	-0.009
	B11	14.4	37.9	37.2	-0.022
	B12	10.7	29.4	29.0	0.001
	B13	8.2	22.6	22.3	0.031
GB697	B14	9.2	21.3	21.1	0.060
	B15	16.7	40.3	39.5	0.013
MC709	B16	23.2	67.9	65.7	-0.001
	B17	22.6	62.7	60.8	-0.030

ω m/yr	$1000\ln^{34}\alpha$= -10‰		$1000\ln^{34}\alpha$= -20‰		$1000\ln^{34}\alpha$= -30‰	
	$^{33}\theta_{modeled}$	$\Delta\Delta^{33}S/\Delta\delta^{34}S$, modeled with $^{33}\theta$=0.51123	$^{33}\theta_{modeled}$	$\Delta\Delta^{33}S/\Delta\delta^{34}S$, modeled with $^{33}\theta$=0.51060	$^{33}\theta_{modeled}$	$\Delta\Delta^{33}S/\Delta\delta^{34}S$, modeled with $^{33}\theta$=0.50996
0	0.5112	-0.00314	0.5106	-0.00314	0.5100	-0.00314
$6*10^{-5}$	0.5112	-0.00314	0.5106	-0.00314	0.100	-0.00314
$6*10^{-4}$	0.5112	-0.00314	0.5106	-0.00314	0.5100	-0.00314
$6*10^{-3}$	0.5112	-0.00314	0.5106	-0.00314	0.5100	-0.00314
$6*10^{-2}$	0.5112	-0.00309	0.5105	-0.00303	0.5098	-0.00298
$6*10^{-1}$	0.5107	-0.00258	0.5095	-0.00200	0.5082	-0.00143
6	0.5106	-0.00252	0.5093	-0.00188	0.5081	-0.00124